ELSEVIER

Chemical Engineering Science 59 (2004) 2297–2313

Chemical Engineering Science

www.elsevier.com/locate/ces

Dynamic modeling of crosslinking and gelation in continuous ethylene–propylene–diene polymerization reactors using the pseudo–kinetic constant approach☆

Rujun Li[a], Armando B. Corripio[a], Kerry M. Dooley[a,*], Michael A. Henson[b], Michael J. Kurtz[c]

[a] *Gordon A. and Mary Cain Department of Chemical Engineering, Louisiana State University, Baton Rouge, LA 70803-7303, USA*
[b] *Department of Chemical Engineering, University of Massachusetts Amherst, 686 N. Pleasant Street, Amherst, MA 01003-3110, USA*
[c] *ExxonMobil Chemical Company, Baton Rouge, LA 70805-3359, USA*

Received 21 March 2003; received in revised form 17 October 2003; accepted 28 January 2004

Abstract

A dynamic model for continuous ethylene–propylene–diene terpolymerization reactors in which crosslinking and gel formation are attributable to reactions between the pendant double bonds of diene units has been developed. The model is applicable to other types of crosslinking reactions such as those due to aging, polymer blending, and vulcanization. The polymer properties at the gel point and in the post-gel region are computed using the numerical fractionation method. Direct application of this method to the prediction of terpolymer properties in the gel or post-gel region can lead to severe numerical problems, due to large differences in order of magnitude of various moments across the generations. These problems are overcome by applying a pseudo-kinetic rate constant method, i.e., by constructing a moment model for a pseudo-homopolymer that approximates the behavior of the actual terpolymer under the long chain and quasi-steady state assumptions. The pseudo-homopolymer model is then used as the basis for application of the numerical fractionation method. We show that the proposed dynamic model is capable of predicting realistic polydispersities and molecular weight distributions even near the gel point with as few as 11 generations, and in the post-gel region with as few as five generations. The largest steady-state polydispersities of the soluble polymer are obtained when the crosslinking rate just exceeds the critical value for gelation. The steady-state polydispersity decreases exponentially in the post-gel region at higher values of the rate constant, while the sol fraction decreases in a more linear fashion. The overall molecular weight distribution (MWD) of the sol is constructed assuming a Schulz two parameter distribution for each generation. For the industrial case of a small number of crosslinks, the first two generations contribute the most to the MWD, which is unimodal. The tail of the MWD is longest near the initial gelation time; the tail is shortened in the post-gel region as higher generations are consumed.

Keywords: Polymerization; Crosslinking; Dynamic simulation; Gels; Kinetics; Numerical fractionation

1. Introduction

Ethylene–propylene (EPM) copolymers and ethylene–propylene–diene (EPDM) terpolymers are used in the manufacturing of automotive components, cable and wire, appliances, building and construction materials and agricultural equipment due to their excellent resistance to ozone and chemicals. Major US producers of EPM and EPDM rubbers include ExxonMobil Chemical, DuPont-Dow, Uniroyal Chemical, DSM Elastomer and Bayer. The annual domestic production of these rubbers in 1995 was almost 400,000 metric tons (Office of Air Quality, EPA, 1995). EPDM is traditionally manufactured via solution polymerization using Ziegler–Natta catalysts. The diene monomer is typically ethylidene norbornene (ENB), although other dienes such as 1,4-hexadiene are also used (ver Strate, 1985; Cozewith, 1988; Noordermeer, 1997). Typical EPDM polymers contain less than 5 wt% diene. Product quality is determined primarily by the Mooney viscosity (a measure of molecular weight), Mooney viscosity relaxation (a measure of polydispersity) and the monomer contents of the polymer. EPDM producers manufacture a variety of

☆ Supplementary data associated with this article can be found in the online version of this article doi: 10.1016/j.ces.2004.01.059.

* Corresponding author. Tel.: +1-225-578-3063; fax: +1-225-578-1476.
E-mail address: dooley@che.lsu.edu (K.M. Dooley).

0009-2509/$ - see front matter © 2004 Elsevier Ltd. All rights reserved.
doi:10.1016/j.ces.2004.01.059

different commercial grades with each grade having different polymer properties. Many grades are composed of linear polymer chains with very little branching. However, some grades include long-chain branches and can contain a gel fraction; polydispersities as high as seven have been measured for weight-average molecular weights in the range 3×10^4–3×10^6 (Cozewith, 1988; Beardsley and Tomlinson, 1990; Saatkamp et al., 1995; Dikland, 1996; Beelen et al., 1998; Pehlert et al., 2001).

In the manufacturing process, gel appears when the degree of crosslinking reaches a certain level. Understanding of gelation and molecular weight distribution of polymer is of importance for polymer manufacturing practice to produce polymers with well-controlled properties. Gel may adversely affect polymer properties. It is difficult to control gel level; runaway gelation can result. Therefore, it is important to understand the gelation mechanism and how to control the level of gel. The gel point (point of incipient gelation) partitions the behavior into pre- and post-gel regions. Population balance-based moment methods are widely used in modeling polymerization processes in the pre-gel region, where all moments are finite and the moment equations can be solved without difficulty. However, at the gel point and in the post-gel region the moment method is no longer capable of representing the system because the second moments go to infinity.

Flory (1953) developed a statistical approach to relate network formation to monomer functionalities and conversions in stepwise polymerizations, but the approach is difficult to apply to addition polymerizations performed in a CSTR (Cozewith and Teymour, 1998). Teymour and Campbell (1994) developed a "numerical fractionation" technique that partitions the polymer network into generations according to the degree of crosslinking. The linear polymer is the zeroth generation, and two zeroth generation polymer chains can crosslink and produce a first-generation polymer chain. In general, an ith generation chain crosslinks with a jth generation chain to produce a chain of: the ith generation if $i > j$; the jth generation if $i < j$; the $(i+1)$th generation if $i = j$. The moment equations for a finite number of generations can be derived. Only the moments of certain lower generations that have a lower degree of crosslinking are calculated. The higher generations are treated as gel. Because each generation has finite second moments, this technique allows integration past the gel point in order to calculate polymer properties in the post-gel region. The physical properties of the soluble polymer (sol) and the weight fraction of the gel can be calculated and the molecular weight distribution of the sol can be reconstructed. This method can be applied to both batch reactors and CSTRs, although the numerical complications are more significant for a CSTR (Cozewith and Teymour, 1998). The method has already been applied to several types of homopolymer batch and CSTR reactors (Arzamendi and Asua, 1995; Topalis et al., 1996; Mazzotti et al., 1996; Pladis and Kiparissides, 1998). The method was also applied to a batch copolymerization reaction by Gossage (1997). However, it has not yet been applied to a copolymerization or terpolymerization in a CSTR. In this paper, the "numerical fractionation" method has been applied to the EPDM terpolymerization process for the first time, and the associated numerical problems have been addressed and solved.

2. Model development

The mechanism of EPDM polymerization without crosslinking used here was first proposed by Cozewith (1988), and is listed in Appendix A. In the mechanism, the addition of a diene unit such as ENB to a propylene-ended chain, and the addition of propylene and diene units to a diene-ended chain, are assumed to be negligible due to the steric hindrance of diene monomer.

An addition to the mechanism proposed by Cozewith et al. (1979) allows for crosslinked chains. This mechanism was originally derived for a homopolymer based on the assumption that two polymer chains can crosslink through the pendant double bonds (PDBs) of the monomers. The mechanism is extended to EPDM terpolymer in this paper. The crosslinking reactions can be represented as follows:

$$D_{i_1 j_1 k_1} + D_{i_2 j_2 k_2} \rightarrow D_{(i_1+i_2)(j_1+j_2)(k_1+k_2-1)}, \quad (1)$$

where D is a dead polymer chain, and i, j, k are the number of ethylene, propylene and reactive PDB units in the chain, respectively. It is assumed that only dead chains can crosslink because the live chains in all cases constitute $< 20\%$ (mole fraction), and usually $< 10\%$, of all chains for the EPDM process discussed in this paper. The crosslinking reaction rate is proportional to the number of PDBs and can be written as

$$r_c = k_c k_1 k_2 D_{i_1 j_1 k_1} D_{i_2 j_2 k_2}, \quad (2)$$

where r_c is the crosslinking reaction rate; k_c is the crosslinking rate constant; and k_1 and k_2 correspond to the number of PDBs in chains 1 and 2, respectively.

The choice of kinetics was motivated by the following. While crosslinking kinetics with cure accelerators such as peroxides or other radical generators, and most long-chain branching kinetics, are typically first order in PDB and first order in live chains (ver Strate et al., 1980; Dikland, 1996; Shaffer and Ray, 1997), the coupling described here requires two PDBs on two different chains. The linkage is initiated by the interaction of a PDB with cocatalyst to form an active (carbenium-ion terminated) branch (Kresge et al., 1985; ver Strate, 1985; Pehlert et al., 2001). However, direct vinylic coupling of PDBs has also been observed, for example in vinyl norbornene homopolymers using $AlEtCl_2$ as catalyst (Kennedy and Makowski, 1967; Dolatkhani et al., 1996). Regardless of the number of intervening links in a branch, the crosslink is not complete until the branch reacts with another PDB. If this last step is rate-limiting, and if intervening branch propagations are at quasi-steady state, a second

order (in PDB) rate expression would result. The total loss of reactive PDBs is then one, because the final reaction does not necessarily terminate the active (carbenium ion) species. However, in the development that follows it will be apparent that we could assume the loss of two reactive PDBs in this process without affecting the simulation results.

Even if the mechanism is not exactly as described here, the second-order kinetics assumption (in PDBs) has been tested to a limited extent by Gardner and ver Strate (1973), who used labeled ENB so they could count both the total number of diene groups by radioassay and refractive index and the number of unreacted PDBs by iodine number. The curve relating the two could be reproduced exactly only by assuming that the amount of consumed PDBs was proportional to the square of the diene content. Also, Dolatkhani et al. (1996) studied the kinetics of homopolymer diene systems, some of which crosslinked. The crosslinking systems were ENB/$VOCl_3$/$AlEt_2Cl$ and ENB/$TiCl_3$/$AlCl_3$. When their crosslinking data are regressed, the overall order in diene is 2, while for the non-crosslinking systems (using dimethyloctadiene) the overall order is ~ 1. NMR and IR spectra showed that direct vinylic coupling occurred for all of the crosslinking systems, with no evidence of vinylic coupling for the other systems. In conclusion, there is solid evidence for second-order kinetics in PDB crosslinking reactions.

Because the number of PDBs equals the number of diene units in the polymer chains if no crosslinking reactions take place, and because typically less than 5% of the PDBs crosslink in a typical EPDM process, it is reasonable to assume that the number of PDBs equals the number of diene units in the polymer chains. This simplification eliminates the need for another set of moments. The following 10 different moments are used to compute the polymer properties. These moments are defined as

Zeroth moment:

$$B_0 = \sum_{i=0}^{\infty}\sum_{j=0}^{\infty}\sum_{k=0}^{\infty} B_{ijk}. \tag{3}$$

B_0 represents the concentration of the dead chains.

First moments:

$$B_{100} = \sum_{i=0}^{\infty}\sum_{j=0}^{\infty}\sum_{k=0}^{\infty} iB_{ijk},$$

$$B_{010} = \sum_{i=0}^{\infty}\sum_{j=0}^{\infty}\sum_{k=0}^{\infty} jB_{ijk},$$

$$B_{001} = \sum_{i=0}^{\infty}\sum_{j=0}^{\infty}\sum_{k=0}^{\infty} kB_{ijk}. \tag{4}$$

B_{100}, B_{010} and B_{001} are the first moments of ethylene, propylene and diene in the dead chains, respectively; they represent the concentrations of the monomers in the dead chains.

Second moments:

$$B_{200} = \sum_{i=0}^{\infty}\sum_{j=0}^{\infty}\sum_{k=0}^{\infty} i^2B_{ijk}, \quad B_{020} = \sum_{i=0}^{\infty}\sum_{j=0}^{\infty}\sum_{k=0}^{\infty} j^2B_{ijk},$$

$$B_{002} = \sum_{i=0}^{\infty}\sum_{j=0}^{\infty}\sum_{k=0}^{\infty} k^2B_{ijk}, \tag{5}$$

$$B_{110} = \sum_{i=0}^{\infty}\sum_{j=0}^{\infty}\sum_{k=0}^{\infty} ijB_{ijk}, \quad B_{101} = \sum_{i=0}^{\infty}\sum_{j=0}^{\infty}\sum_{k=0}^{\infty} ikB_{ijk},$$

$$B_{011} = \sum_{i=0}^{\infty}\sum_{j=0}^{\infty}\sum_{k=0}^{\infty} jkB_{ijk}. \tag{6}$$

B_{200}, B_{020}, B_{002}, B_{110}, B_{101} and B_{011} are the six individual second moments of the dead chains with respect to ethylene alone, propylene alone, diene alone, ethylene and propylene, ethylene and diene, and propylene and diene, respectively. The second moments do not have an explicit physical interpretation. From these moments, we can compute the monomer content, number and weight average molecular weights and polydispersity of the polymer. The moment equations themselves are provided as supplementary material.

The contribution of the crosslinking reaction to the moment equations is as follows:

Zeroth moment:

$$r_{c,B_0} = -\frac{1}{2}k_c(B_{001})^2. \tag{7}$$

First moments:

$$r_{c,B_{100}} = 0, \tag{8}$$

$$r_{c,B_{010}} = 0, \tag{9}$$

$$r_{c,B_{001}} = 0. \tag{10}$$

Second moments:

$$r_{c,B_{200}} = k_c(B_{101})^2, \tag{11}$$

$$r_{c,B_{020}} = k_c(B_{011})^2, \tag{12}$$

$$r_{c,B_{002}} = k_c(B_{002})^2, \tag{13}$$

$$r_{c,B_{101}} = k_cB_{002}B_{101}, \tag{14}$$

$$r_{c,B_{011}} = k_cB_{002}B_{011}, \tag{15}$$

$$r_{c,B_{110}} = k_cB_{101}B_{011}. \tag{16}$$

This model includes 35 state variables: concentrations of the three monomers, the inactive and active forms of the catalyst, the alkyl co-catalyst, and hydrogen (chain transfer agent); and four zeroth moments, 12 first moments and 12 second moments. This will be referred to as "the full model" in contrast to a reduced model derived using a pseudo-kinetic constant approach.

The gel point is critical to polymer property control because gel can adversely affect the rheological and other polymer properties. The degree of the crosslinking must be well-controlled to avoid formation of gel or to maintain the mass fraction of gel below a certain level. Mathematically, gel is characterized by infinite weight average molecular weight and second moments. The critical k_c is the minimum value of k_c that allows gel to form under the given feed conditions. To focus on the dynamic effects of crosslinking, we assume in agreement with observation that crosslinking reactions take place over a much longer time scale than chain propagation (Cozewith and Teymour, 1998), so we can assume that the linear chains are in quasi-steady state. We then write a moment equation for the second moment with respect to diene in a CSTR, prior to or in the absence of crosslinking.

$$\frac{dB_{002,L}}{dt} = -\frac{1}{\theta} B_{002,L} + r_{p,B_{002,L}} = 0, \tag{17}$$

where $B_{002,L}$ is a second moment for the purely linear polymer prior to or in the absence of crosslinking, $r_{p,B_{002,L}}$ is the generation rate of $B_{002,L}$, and θ is the residence time. Given the much longer time scale for crosslinking, the ODE for the second moment with respect to diene when crosslinking does take place becomes:

$$\begin{aligned}\frac{dB_{002}}{dt} &= -\frac{1}{\theta} B_{002} + r_{p,B_{002,L}} + k_c (B_{002})^2 \\ &= \frac{1}{\theta}(B_{002,L} - B_{002}) + k_c (B_{002})^2. \end{aligned} \tag{18}$$

To guarantee that B_{002} will be finite and real, the following inequality must hold at steady state:

$$k_c \leqslant \frac{1}{4\theta B_{002,L}}. \tag{19}$$

As k_c increases, B_{002} eventually becomes infinite, causing the other five second moments to simultaneously become infinite and indicating that gel is formed. The value $\frac{1}{4\theta B_{002,L}}$ is called the critical k_c ($k_{c,c}$). The critical residence time (θ_c) can be calculated as

$$\theta_c = \frac{1}{4k_{c,c} B_{002,L}}. \tag{20}$$

This represents the minimum residence time at which gel could form in a CSTR.

3. Pseudo-kinetic constant approach for crosslinking reactions

Because the typical moment method is only valid in the pre-gel region, Teymour and Campbell (1994) proposed a "numerical fractionation" method that allows integration of the moment equations up to and through the gel point, in order to compute distributions in the post-gel region. Cozewith and Teymour (1998) noticed that the numerical fractionation approach exhibits numerical difficulties in the calculation of homopolymer moments in a CSTR due to large differences in the order of magnitude of moments across generations and accumulated errors for those moments near zero. We first applied the method directly to the EPDM terpolymerization in a CSTR. The moment equations for the crosslinking reactions are as follows.

Zeroth moment

$$\begin{aligned}\frac{dg_{m,0}}{dt} &= k_c g_{m,001} \sum_{n=0}^{m-1} g_{n,001} \\ &\quad + \frac{k_c}{2} (g_{m-1,001})^2 - k_c g_{m,001} B_{001}. \end{aligned} \tag{21}$$

First moments

$$\begin{aligned}\frac{dg_{m,100}}{dt} &= k_c \left(g_{m,101} \sum_{n=0}^{m-1} g_{n,001} + g_{m,001} \sum_{n=0}^{m-1} g_{n,101} \right) \\ &\quad + k_c g_{m-1,101} g_{m-1,001} - k_c g_{m,101} B_{001}, \end{aligned} \tag{22}$$

$$\begin{aligned}\frac{dg_{m,010}}{dt} &= k_c \left(g_{m,011} \sum_{n=0}^{m-1} g_{n,001} + g_{m,001} \sum_{n=0}^{m-1} g_{n,011} \right) \\ &\quad + k_c g_{m-1,011} g_{m-1,001} - k_c g_{m,011} B_{001}, \end{aligned} \tag{23}$$

$$\begin{aligned}\frac{dg_{m,001}}{dt} &= k_c \left(g_{m,002} \sum_{n=0}^{m-1} g_{n,001} + g_{m,001} \sum_{n=0}^{m-1} g_{n,002} \right) \\ &\quad + k_c g_{m-1,002} g_{m-1,001} - k_c g_{m,002} B_{001}. \end{aligned} \tag{24}$$

Second moments

$$\begin{aligned}\frac{dg_{m,200}}{dt} &= k_c \left(g_{m,201} \sum_{n=0}^{m-1} g_{n,001} + 2 g_{m,101} \sum_{n=0}^{m-1} g_{n,101} \right. \\ &\quad \left. + g_{m,001} \sum_{n=0}^{m-1} g_{n,201} \right) + k_c g_{m-1,201} g_{m-1,001} \\ &\quad + k_c (g_{m-1,101})^2 - k_c g_{m,201} B_{001}, \end{aligned} \tag{25}$$

$$\begin{aligned}\frac{dg_{m,020}}{dt} &= k_c \left(g_{m,021} \sum_{n=0}^{m-1} g_{n,001} + 2 g_{m,011} \sum_{n=0}^{m-1} g_{n,011} \right. \\ &\quad \left. + g_{m,001} \sum_{n=0}^{m-1} g_{n,021} \right) + k_c g_{m-1,021} g_{m-1,001} \\ &\quad + k_c (g_{m-1,011})^2 - k_c g_{m,021} B_{001}, \end{aligned} \tag{26}$$

$$\begin{aligned}\frac{dg_{m,002}}{dt} &= k_c \left(g_{m,003} \sum_{n=0}^{m-1} g_{n,001} + 2 g_{m,002} \sum_{n=0}^{m-1} g_{n,002} \right. \\ &\quad \left. + g_{m,001} \sum_{n=0}^{m-1} g_{n,003} \right) + k_c g_{m-1,003} g_{m-1,001} \\ &\quad + k_c (g_{m-1,002})^2 - k_c g_{m,003} B_{001}, \end{aligned} \tag{27}$$

$$\frac{dg_{m,110}}{dt} = k_c \left(g_{m,111} \sum_{n=0}^{m-1} g_{n,001} + g_{m,101} \sum_{n=0}^{m-1} g_{n,011} + g_{m,011} \sum_{n=0}^{m-1} g_{n,101} + g_{m,001} \sum_{n=0}^{m-1} g_{n,111} \right) + k_c g_{m-1,111} g_{m-1,001} + k_c g_{m-1,101} g_{m-1,011} - k_c g_{m,111} B_{001}, \quad (28)$$

$$\frac{dg_{m,101}}{dt} = k_c \left(g_{m,102} \sum_{n=0}^{m-1} g_{n,001} + g_{m,101} \sum_{n=0}^{m-1} g_{n,002} + g_{m,002} \sum_{n=0}^{m-1} g_{n,101} + g_{m,001} \sum_{n=0}^{m-1} g_{n,102} \right) + k_c g_{m-1,102} g_{m-1,001} + k_c g_{m-1,101} g_{m-1,002} - k_c g_{m,102} B_{001}, \quad (29)$$

$$\frac{dg_{m,011}}{dt} = k_c \left(g_{m,012} \sum_{n=0}^{m-1} g_{n,001} + g_{m,011} \sum_{n=0}^{m-1} g_{n,002} + g_{m,002} \sum_{n=0}^{m-1} g_{n,011} + g_{m,001} \sum_{n=0}^{m-1} g_{n,012} \right) + k_c g_{m-1,012} g_{m-1,001} + k_c g_{m-1,011} g_{m-1,002} - k_c g_{m,012} B_{001}. \quad (30)$$

In these equations, g represents moments, and m represents generations. The above equations constitute the general form for the first and higher generations. For the zeroth moments, only the consumption terms appear in the equations. Note that in the second moment equation the third moments also appear, as in the full model. This non-closure problem was addressed in both cases using a closure approximation (Saidel and Katz, 1968), as shown in

$$g_{m,3} = \frac{2g_{m,2}^2}{g_{m,1}} - \frac{g_{m,2} g_{m,1}}{g_0}. \quad (31)$$

Because the closure approximation only involves bulk moments, the long-chain assumption was used to obtain the individual third moments. This assumption assumes that the chains are long enough that all chains have identical monomer contents. The individual third moments were computed from the long-chain assumption under which the following equations can be derived (the colons in Eq. (32) denote ratios):

$$\begin{aligned} &g_{m,200} : g_{m,020} : g_{m,002} : g_{m,110} : g_{m,101} : g_{m,011} \\ &\quad = (g_{m,100})^2 : (g_{m,010})^2 : (g_{m,001})^2 : g_{m,100} g_{m,010} \\ &\quad : g_{m,100} g_{m,001} : g_{m,010} g_{m,001}, \end{aligned} \quad (32)$$

$$\begin{aligned} &g_{300,m} : g_{030,m} : g_{m,003} : g_{210,m} : g_{m,201} : g_{120,m} : g_{m,021} \\ &\quad : g_{m,102} : g_{m,012} : g_{m,111} \\ &\quad = (g_{m,100})^3 : (g_{m,010})^3 : (g_{m,001})^3 : (g_{m,100})^2 g_{m,010} \\ &\quad : (g_{m,100})^2 g_{m,001} : g_{m,100} (g_{m,010})^2 \\ &\quad : (g_{m,010})^2 g_{m,001} : g_{m,100} (g_{m,001})^2 : g_{m,010} (g_{m,001})^2 \\ &\quad : g_{m,100} g_{m,010} g_{m,001}. \end{aligned} \quad (33)$$

The bulk moments of a generation are given in terms of the individual generational moments as follows:

$$g_{m,1} = g_{m,100} + g_{m,010} + g_{m,001}, \quad (34)$$

$$g_{m,2} = g_{m,200} + g_{m,020} + g_{m,002} + 2g_{m,110} + 2g_{m,101} + 2g_{m,011}, \quad (35)$$

$$g_{m,3} = g_{m,300} + g_{m,030} + g_{m,003} + 3g_{m,210} + 3g_{m,201} + 3g_{m,120} + 3g_{m,021} + 3g_{m,102} + 3g_{m,012} + 6g_{m,111}. \quad (36)$$

From Eqs. (33)–(36), we can compute the individual third moments and solve the ODEs for the zeroth, first and second moments for each generation. However, when we applied the numerical fractionation method to the EPDM process, even larger differences in the magnitudes of moments within and across generations than those of homopolymer were observed. Typical ODE solvers were not able to converge the moments of higher generations. Therefore, the pseudo-kinetic constant approach was used to simplify the terpolymer to a pseudo-homopolymer, and then the numerical fractionation approach was applied to the pseudo-homopolymer system.

This pseudo-kinetic constant approach (Xie and Hamielec, 1993a,b,c) has been widely used in the modeling of free-radical polymerization. The approach is based on a quasi-steady state assumption for both the free radicals and the live chains. The concentrations of the pseudo-monomer (C_M) and pseudo-live polymer (L_0) are defined as the sum of the concentrations of the monomers and live polymer chains, respectively:

$$C_M = \sum_{i=1}^{3} C_{M_i}, \quad (37)$$

$$L_0 = P_0 + Q_0 + R_0, \quad (38)$$

where C_{M_i} is the concentration of the ith monomer and P_0, Q_0 and R_0 are the concentrations of ethylene-, propylene- and diene-ended live polymer chains, respectively. The mole fraction of each monomer (Φ_{M_i}) is calculated as

$$\Phi_{M_i} = \frac{C_{M_i}}{C_M}. \quad (39)$$

The mole fractions of individual polymer chains are calculated from equations derived using the quasi-steady-state assumption, i.e., the overall contents of chains are in steady state:

$$k_{12}P_0C_{M_2} = k_{21}Q_0C_{M_1}, \tag{40}$$

$$k_{13}P_0C_{M_3} = k_{31}R_0C_{M_1}. \tag{41}$$

Therefore, the monomer contents of the chains are functions of both propagation rate constants and monomer concentrations:

$$\Phi_P = \frac{P_0}{L_0} = \frac{1}{1 + \dfrac{k_{12}C_{M_2}}{k_{21}C_{M_1}} + \dfrac{k_{13}C_{M_3}}{k_{31}C_{M_1}}}, \tag{42}$$

$$\Phi_Q = \frac{Q_0}{L_0} = \frac{k_{12}C_{M_2}}{k_{21}C_{M_1}}\Phi_P, \tag{43}$$

$$\Phi_R = 1 - \frac{P_0}{L_0} - \frac{Q_0}{L_0} = 1 - \Phi_P - \Phi_Q. \tag{44}$$

The pseudo-propagation rate constant k_p can be defined as

$$k_p = (k_{11}\Phi_P + k_{21}\Phi_Q + k_{31}\Phi_R)\Phi_{M_1} + (k_{12}\Phi_P + k_{22}\Phi_Q)\Phi_{M_2} + k_{13}\Phi_P\Phi_{M_3} \tag{45}$$

and the propagation reaction rate can be written as follows:

$$r_p = k_pC_ML_0. \tag{46}$$

The crosslinking reaction of the terpolymer (Eq. (1)) is simplified as

$$D_{r_1l_1} + D_{r_2l_2} \rightarrow D_{(r_1+r_2)(l_1+l_2-1)}, \tag{47}$$

where r is the number of total monomer units and l is the number of PDBs in the chain. The crosslinking reaction terms of the dead chains can now be written as

$$r_{c,B_0} = -\frac{1}{2}k_c(\mathrm{PDB})^2, \tag{48}$$

$$r_{c,B_1} = 0, \tag{49}$$

$$r_{c,B_2} = k_c\left(\sum_{r=1}^{\infty}\sum_{l=1}^{\infty} rlB_{rl}\right)^2, \tag{50}$$

where PDB is the overall concentration of PDBs, and B_0, B_1 and B_2 are the bulk zeroth, first and second moments of the dead pseudo-homopolymer, respectively. The loss of one (or more) PDBs can be ignored in the derivation because the number of crosslinked PDBs for the polymers of interest is very small compared to the overall PDB concentration. The first and second moments of the pseudo-homopolymer are the sums of the individual first and second moments (Ogunnaike, 1994):

$$B_1 = B_{100} + B_{010} + B_{001}, \tag{51}$$

$$B_2 = B_{200} + B_{020} + B_{002} + 2B_{110} + 2B_{101} + 2B_{011}. \tag{52}$$

The term $\sum_{r=1}^{\infty}\sum_{l=1}^{\infty} rlB_{rl}$ in Eq. (50) is a cross second moment and gives rise to a non-closure problem because higher-order moments are required to solve the equations. To avoid this problem a long-chain assumption is invoked (Gossage, 1997); all chains in the reactor are assumed long enough that their monomer contents are identical. Therefore, the ratios of numbers of individual monomers in each chain equal the ratios of their associated first moments. Let Φ_{PDB} be the fraction of PDBs in the dead chains:

$$\Phi_{\mathrm{PDB}} = \frac{l}{r} = \frac{\mathrm{PDB}}{B_1}. \tag{53}$$

Then Eq. (50) can be written as

$$\frac{\mathrm{d}B_2}{\mathrm{d}t} = k_c(\Phi_{\mathrm{PDB}}B_2)^2. \tag{54}$$

This reduced model has 15 state variables with the first seven states the same as the full model. The other state variables are: two bulk zeroth moments (live and dead), two bulk first moments (live and dead), two bulk second moments (live and dead), and the PDB concentrations in live and dead chains. The detailed ODEs for the reduced model are listed in Appendix B. Because the moments in the reduced model are not based on the individual monomers, there are no large differences in the order of magnitude of moments within and across generations as in the full model. Therefore, we can use the numerical fractionation approach to calculate the polymer properties in the post-gel region. When the numerical fractionation approach is applied to the pseudo-homopolymer, the fraction of PDBs for each generation (Φ_{PDB_m}) can be assumed to equal the overall PDB fraction because the crosslinking density is low:

$$\Phi_{\mathrm{PDB}_m} = \frac{\mathrm{PDB}_m}{g_{m,1}} = \frac{\mathrm{PDB}}{B_1}, \tag{55}$$

where $g_{m,1}$ denotes the first moment of the mth generation. Then the moments of the crosslinking reactions for each generation can be written as

$$\frac{\mathrm{d}g_{m,0}}{\mathrm{d}t} = -k_c\Phi_{\mathrm{PDB}}g_{m,1}\mathrm{PDB} \quad (m = 0), \tag{56}$$

$$\frac{\mathrm{d}g_{m,0}}{\mathrm{d}t} = k_c\Phi_{\mathrm{PDB}}^2\left[g_{m,1}\sum_{n=0}^{m-1}g_{n,1} + \frac{1}{2}(g_{m-1,1})^2\right] - k_c\Phi_{\mathrm{PDB}}g_{m,1}\mathrm{PDB} \quad (m \geqslant 1), \tag{57}$$

$$\frac{\mathrm{d}g_{m,1}}{\mathrm{d}t} = -k_c\Phi_{\mathrm{PDB}}g_{m,2}\mathrm{PDB} \quad (m = 0), \tag{58}$$

$$\frac{\mathrm{d}g_{m,1}}{\mathrm{d}t} = k_c\Phi_{\mathrm{PDB}}^2\left(g_{m,2}\sum_{n=0}^{m-1}g_{n,1} + g_{m,1}\sum_{n=0}^{m-1}g_{n,2}\right) + k_cg_{m-1,2}g_{m-1,1} - k_c\Phi_{\mathrm{PDB}} g_{m,2}\mathrm{PDB} \quad (m \geqslant 1), \tag{59}$$

$$\frac{dg_{m,2}}{dt} = -k_c \Phi_{PDB} g_{m,3} PDB \quad (m = 0), \tag{60}$$

$$\frac{dg_{m,2}}{dt} = k_c \Phi_{PDB}^2 \left(g_{m,3} \sum_{n=0}^{m-1} g_{n,1} + 2 g_{m,2} \sum_{n=0}^{m-1} g_{n,2} + g_{m,1} \sum_{n=0}^{m-1} g_{n,3} \right) + k_c \Phi_{PDB}^2 (g_{m-1,3} g_{m-1,1} + g_{m-1,2}^2) - k_c \Phi_{PDB} g_{m,3} PDB \quad (m \geqslant 1). \tag{61}$$

Note that in the second moment equation third moments appear, as in the full model. This non-closure problem is solved using the same closure approximation (Saidel and Katz, 1968) as shown in Eq. (31).

Gossage (1997) has shown that the molecular weight distribution computed using the numerical fractionation method showed good agreement with experimental data, and the crosslinking density computed by the numerical fractionation method for a batch reactor agrees with Flory's theory. Papavasiliou et al. (2002) compared the reconstructed MWD using this closure with the direct solution, and showed that the closure can cause large errors in the MWD. Comparison was also made for the EPDM process and the results will be shown in the following section.

4. Results and discussion

4.1. Computational issues

Dynamic simulations were performed using Matlab and Simulink. The ODE solver used was "ode23tb", an implicit Runge–Kutta formulation with two stages. The first stage is a trapezoidal rule step and the second stage is a backward difference formula of order two. This solver has been demonstrated to solve stiff problems efficiently (Bank et al., 1985; Shampine and Hosea, 1996). The numerical fractionation method overcomes the problems of the traditional moment method at the gel point, and is able to continue the calculations into the post-gel region. But the method requires very high accuracy for the moments of the higher generations. When it is applied to the full model, large differences in magnitudes of different moments within the same generation and across different generations resulted in serious computational problems. In particular, the ODE solver failed to converge in the post-gel region where certain generations disappeared. When the method is applied to the reduced model, differences in magnitudes of the moments are reduced by collapsing the individual first and second moments into the bulk moments. Even so the integration requires stringent tolerances. The absolute tolerance was set to 10^{-14} and the relative tolerance to 10^{-8} to achieve convergence at all conditions tested. The default values for the tolerances are 10^{-6} and 10^{-3}, respectively. The CPU time for a 10-h simulation with 11 generations, feed conditions as listed in the following section, and $k_c = 3.12 k_{c,c}$ was about 10 min on a PC with a Pentium IV 1.70 GHz processor and 128 MB memory. The CPU time for the same simulation with only one generation is less than 20 s.

4.2. Validation of the assumptions

There are three major approximations used in deriving the pseudo-kinetic model within the numerical fractionation framework: the quasi-steady-state assumption, the long-chain assumption, and the third moment approximation. The quasi-steady-state assumption simplifies the terpolymer to a pseudo-homopolymer and reduces the full model with 35 state variables to the reduced model with 15 state variables. The long-chain assumption makes the numerical fractionation method applicable to the reduced model, and is used exclusively for the crosslinking reactions. The third moment approximation allows the third moment to be calculated from the three lower-order moments for solving the second moment equations. In this section, the first two assumptions are tested. The validity of the third assumption has been discussed extensively by Cozewith and Teymour (1998), and is also considered in a later section. Potential errors arising from an inadequate number of generations are also considered here.

The derivation of the reduced model equations themselves, with $k_c = 0$, was checked by comparing their solution to the chain length distribution for a CSTR at steady state, which can be obtained from simple exit-age distribution considerations. First, the full model was solved at steady state for P, Q, R, M_1, M_2, and M_3. The number chain length distributions for P, Q, and R were generated by multiplying the exit-age distribution by the solutions of the age equations (e.g., for M_1):

$$\frac{dx_{M_1}(t)}{dt} = \frac{(k_{11}P_0 + k_{21}Q_0 + k_{31}R_0)C_{M_1} - (k_t + k_{t_2}C_{M_2} + k_{t_3}C_{M_3})(P_{100} + Q_{100} + R_{100})}{P_0 + Q_0 + R_0} = r_{M_1}(\theta). \tag{62}$$

With similar equations for x_{M_2} and x_{M_3}. In other words, the vessel was assumed to be perfectly macromixed with no micromixing. Under these conditions, $x(t) = [r(\theta)]t$, so using the weight fraction:

$$W(t) = \frac{x(t)\frac{dE(t)}{dt}}{\int_0^\infty x(t)\frac{dE(t)}{dt}dt}. \tag{63}$$

Upon substitution for $x(t)$ and $E(t)$, if $r(\theta)$ is defined as the sum of the dimensionless polymerization rates for all

Table 1
Scaled reaction rate constants[a]

Parameter	Value	Parameter	Value
k_a	0.3663	k_{21}	0.6410
k_x	0	k_{22}	3.0037
k_{x_2}	0	k_{31}	1.2418
k_{x_3}	0.9890	k_t	0.5604
k_{i1}	1.8315	k_{t_2}	0.7839
k_{i2}	1.8315	k_{t_3}	0
k_{11}	0.4212	k_{tr}	0
k_{12}	0.6886	k_{tr_1}	1.7582
k_{13}	0.4139	$k_{tr_{M_2}}$	1

[a]Parameters were first scaled to the range of 1–10 and then divided by the scaled value of $k_{tr_{M_2}}$.

monomers, the following equation for weight chain length distribution results:

$$W(x) = \frac{x}{\theta^2 r^2(\theta)} \, \mathrm{e}^{-x/\theta r(\theta)}. \tag{64}$$

This solution is independent of the structure of the moment equations. We compared number- and weight-average chain lengths computed using these equations to those computed from the steady-state equations of the reduced model in Appendix B, $k_c = 0$. Average relative deviations using the kinetics constants of Table 1 were less than 1% in the number average chain length and less than 5% in a typical $W(x)$ with chain transfer reactions included (less than 1% for no chain transfer, where the long-chain assumption is better satisfied). Therefore, the moment calculations of the reduced model are valid, at least in the limit of no crosslinking.

4.2.1. Validation of the quasi-steady-state assumption

Xie and Hamielec (1993a–c) point out that the relative error caused by this assumption is a function of the average molecular weights. The larger the number or weight average molecular weight, the smaller the error. The "quasi-steady-state" assumption was tested under startup conditions again using a EPDM system that does not crosslink. Both the full model and reduced model were simulated using the same set of kinetic parameters. The predicted $\bar{M}_n$ and $\bar{M}_w$ by the reduced model were compared with those of the full model for the errors introduced by the assumption. The scaled parameter values are listed in Table 1. The parameter values are scaled for proprietary reasons. The kinetic parameter set used in this paper predicts average molecular weights greater than 10^2 kg/mol. The maximum relative dynamic errors in $\bar{M}_n$ and $\bar{M}_w$ resulting from the assumption are 4×10^{-3}% and 2.2%, respectively, both of which are smaller than the measurement error. To check the effect of the assumption at lower molecular weights, the H_2 chain transfer reaction constant (k_{tr_1}) was increased to produce lower molecular weight polymer. The simulation results show that even when k_{tr_1} is 1000 times larger than the nominal value and the average molecular weights are reduced to approximately 20% of their original values, the relative errors are still roughly the same magnitudes. The errors for different k_{tr_1} values are listed in Table 2.

4.2.2. Validation of the long-chain assumption

The long-chain assumption was tested at steady state using a terpolymer system with crosslinking reactions in the pre-gel region. For k_c values ranging from zero to just below the critical k_c, the full and reduced models were compared, by analyzing the relative error of B_{002} in the reduced model using the long-chain assumption. The crosslinking constant can be varied in practice by either the use of different crosslinking inhibitors and/or by varying the cocatalyst/catalyst ratio (Kresge et al., 1985; ver Strate, 1985). If the long-chain assumption holds exactly then the following equation is obtained:

$$\left(\frac{\mathrm{PDB}}{B_1}\right)^2 = \frac{B_{002}}{B_2}. \tag{65}$$

The relative error due to the assumption is expressed as $1 - \frac{(\mathrm{PDB}/B_1)^2}{B_{002}/B_2}$ and plotted against k_c in Fig. 1. As k_c increases from zero to near the critical value, the absolute value of the error increases from about 1.5% to 2.3%. When k_c is small the polymer is composed mainly of linear chains; as k_c increases, branched chains whose second moment ratios differ from those of linear chains begin to appear. From Fig. 1 we can see that the second moment is underestimated; therefore, this approximation will underestimate polydispersity as well. The relative error in the polydispersity predicted by the pseudo-kinetic model is plotted in Fig. 2. The error increases as k_c increases, accelerating rapidly as k_c approaches the critical value. Simulation results show that the critical k_c is 1.60 in the full model, and 1.65 in the pseudo-kinetic model. In conclusion, this assumption will cause errors near the gel point. But in the post-gel region the highly crosslinked chains are quickly consumed as gel, so the polydispersity of the sol decreases and linear chains dominate the soluble polymer once again. Therefore, the error is expected to

Table 2
Errors caused by the quasi-steady-state assumption

k_{tr_1} value (ratio to the original value)		1	10	100	1000
Error (%)	$\bar{M}_n$	-4×10^{-3}	-4.4×10^{-3}	-2×10^{-2}	-1.1×10^{-3}
	$\bar{M}_w$	-2.2	-2.25	-1.9×10^{-1}	8.6×10^{-1}

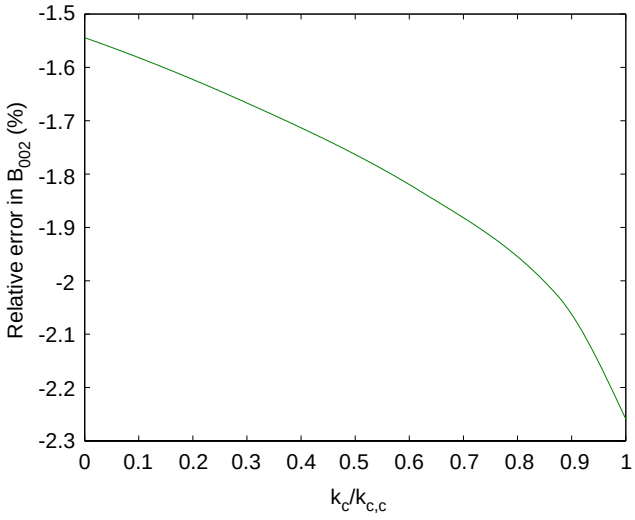

Fig. 1. Relative error in B_{002} caused by crosslinking in the pre-gel region.

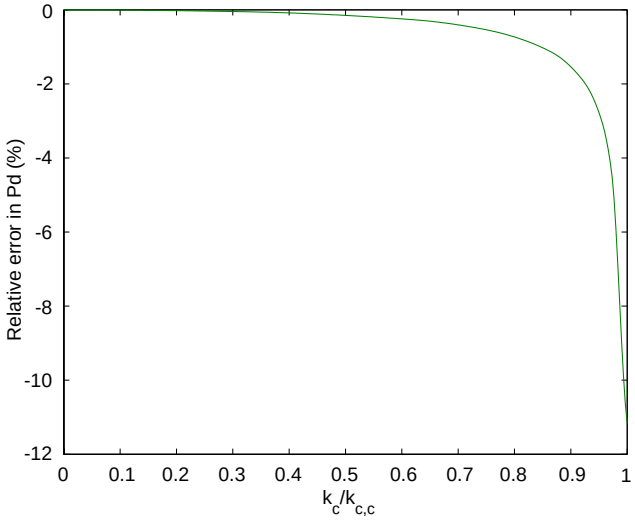

Fig. 2. Relative error in polydispersity in the pre-gel region.

rapidly decrease in the post-gel region. Unfortunately, the error cannot be estimated in the post-gel region because the full model cannot be reliably solved when $k_c > k_{c,c}$.

4.2.3. Error caused by the number of generations

In the numerical fractionation method, the generations included in the model are treated as soluble polymer. Higher generations not included are considered to be gel. All the generations used in the model have finite second moments and finite polydispersity. Therefore, the model requires an infinite number of generations to reproduce the behavior of the polymer at the gel point where the polydispersity becomes infinite. The numerical fractionation method will generate potentially large errors in the neighborhood of the gel point. By contrast, in the post-gel region the higher generations are consumed quickly and the polydispersity of the sol decreases dramatically. The number of generations used

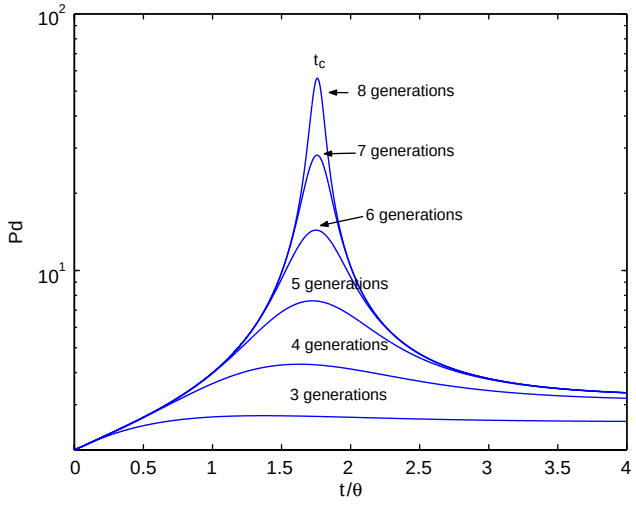

Fig. 3. Evolution of the polydispersity for different numbers of generations when $k_c = 3.12k_{c,c}$.

represents a tradeoff between accuracy near the gel point and computational efficiency and reliability.

The following dynamics simulation was performed to determine an acceptable tradeoff. The initial condition was the steady-state solution of the full model without crosslinking reactions. The crosslinking reactions ($k_c = 3.12k_{c,c}$) began at time zero. This test was designed to study the dynamics of crosslinking and the characteristics of the numerical fractionation approach without interference from the other reactions. It is justified given the very different characteristic time scales of the propagation reactions relative to the crosslinking reactions. Fig. 3 shows results for the evolution of the polydispersity from pre-gel to final steady state at the same feed conditions as in Figs. 1 and 2. Note that the polydispersity is two at time zero because the linear polymer follows the most probable distribution. The dynamics of gelation are faithfully represented in the post-gel region, and the final steady state is accurately predicted, with as few as five (zeroth to fourth) generations. However, more generations are required to accurately represent the dynamics near the gel point. The required number of generations for this region was determined by successively adding generations until the predicted polydispersities in Fig. 3 were constant in the time range $(1 \pm 0.025)t_c$ range, where t_c is the gel time. Simulations using different k_c values within a reasonable range for the EPDM process ($k_c/k_{c,c} = 0.1$-6), showed that 11 total generations are adequate to approximate the dynamics near the gel point, and the computational demands are not excessive.

4.3. Dynamics of crosslinking reactions in the post-gel region

The evolution of the bulk second moments was analyzed first, because the second moments are closely associated

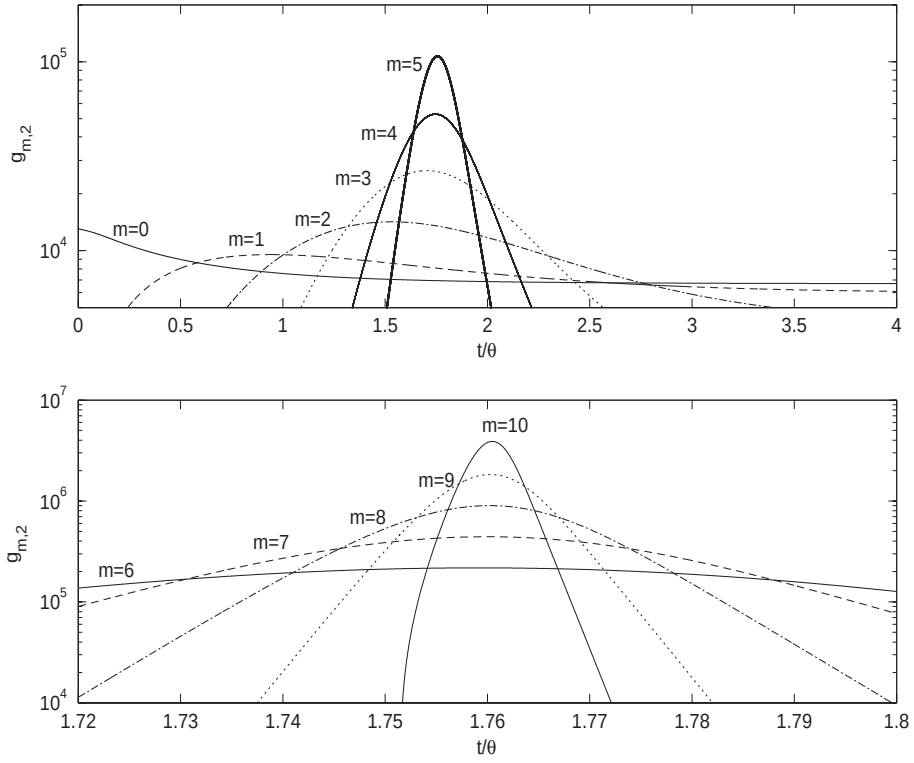

Fig. 4. Evolution of second moments of the individual generations in the post-gel region.

with the formation of gel. We found that the second moments of different generations evolve very differently in the post-gel region (Fig. 4). The linear polymer (zeroth generation) decreases slowly from its initial value to its new steady state. The first through third generations show similar behavior, increasing from zero to their maxima which occur prior to the gel point, then decreasing to nonzero steady-state values. The lower the generation, the earlier in time the maximum occurs. The higher generations increase to their maximum values at the gel point and then decrease to zero. We can also see that the higher the generation, the faster the dynamics associated with crosslinking. When gel is formed, the higher generations begin to decrease at the gel point because the sol consumption rate by the gel ($-k_c\Phi_{\mathrm{PDB}}^2 g_{m,1}\sum_{n=m}^{\infty} g_n$) is larger than the sol production rate by the lower generations ($\frac{1}{2}k_c(g_{m-1,1})^2$). Because the higher generations have higher degrees of crosslinking, they are consumed faster and come to the zero steady state more rapidly. As a result, the polydispersity decreases rapidly after the gel point and reaches the steady state shown in Fig. 5.

In the post-gel region, the polymer is composed of both sol and gel. The mass fraction of sol (x_{sol}) is calculated as the ratio of the sum of first moments of all the generations and the first moment of the polymer:

$$x_{\mathrm{sol}} = \frac{\sum_{m=0}^{M} g_{m,1} + L_1}{B_1 + L_1}, \tag{66}$$

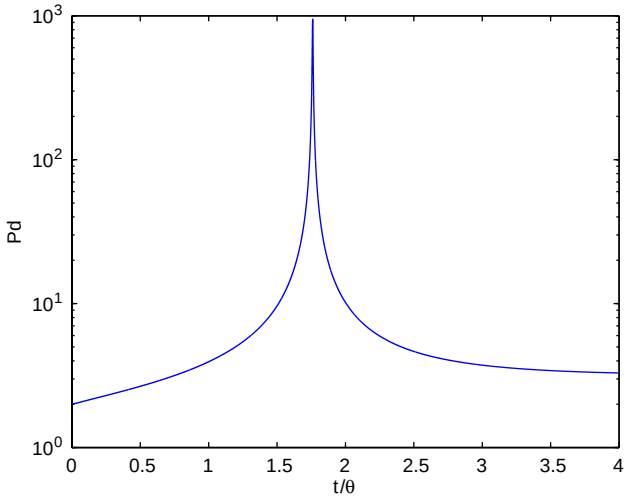

Fig. 5. Evolution of overall polydispersity in the pre- and post-gel regions.

where M is the highest generation used. In the manufacturing practice, crosslinking inhibitors, type of cocatalyst, and the cocatalyst/catalyst ratio control crosslinking, and so the gel fraction. The effects are complex; the simplest way to model them is to vary the crosslinking rate constant. The residence time was not varied in the simulations because in manufacturing practice the residence time is kept relatively constant. Fig. 6 shows the evolution of the sol fraction at $\frac{k_c}{k_{c,c}}$ = 1.88, 3.12 and 4.38. A smaller k_c not only results in less

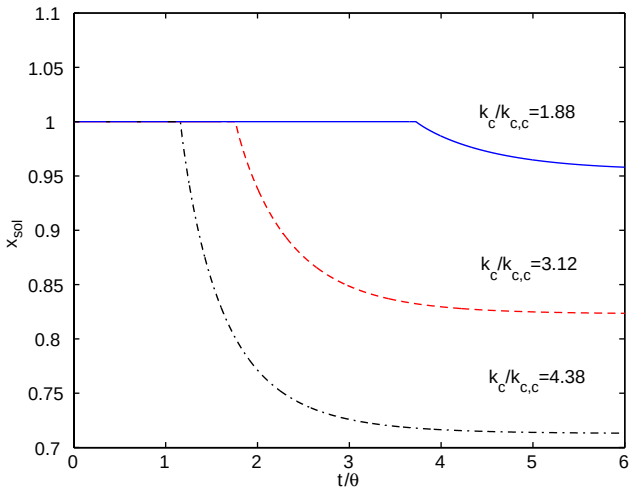

Fig. 6. Evolution of the sol fraction in the post-gel region.

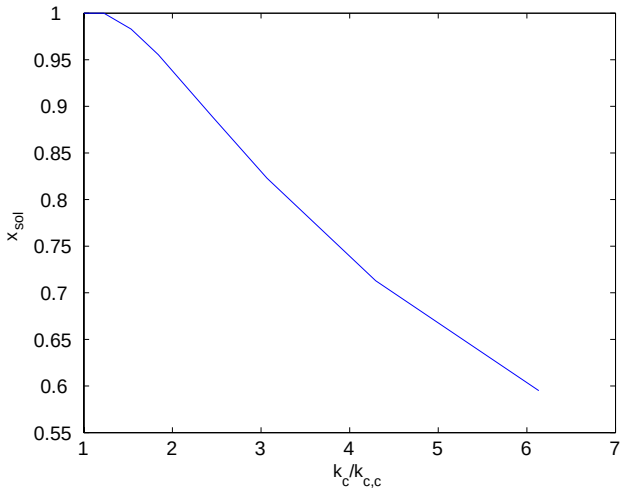

Fig. 8. Steady-state sol fraction in the post-gel region.

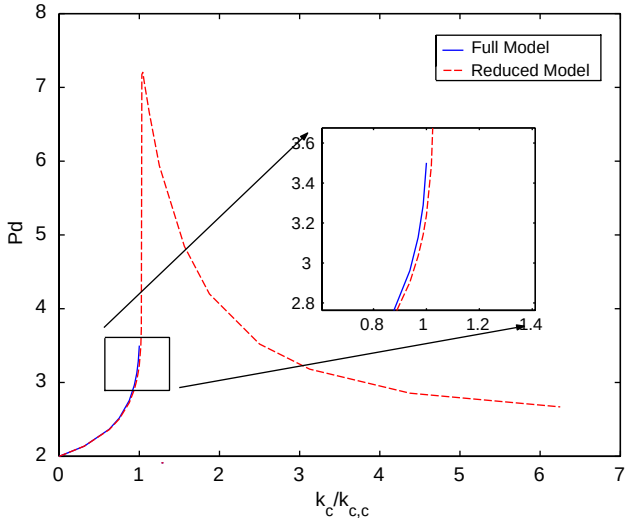

Fig. 7. Steady-state polydispersity in the pre- and post-gel regions.

gel, but also causes the sol to approach steady state more slowly. Figs. 7 and 8 show the steady-state polydispersity of the sol and the sol fraction, respectively, as functions of k_c. Note that the range of polydispersities in Fig. 7, from two to slightly greater than seven, is typical of crosslinked EPDM (Beardsley and Tomlinson, 1990; Saatkamp et al., 1995; Beelen et al., 1998; Pehlert et al., 2001). The maximum steady-state polydispersity is close in value to the literature value of 6.6 (Beelen et al., 1998). A large polydispersity in the post-gel region is obtained when k_c just exceeds the critical value. As k_c increases, the steady-state polydispersity of the sol in the post-gel region decreases almost exponentially. The sol fraction, on the other hand, decreases with k_c in a more linear fashion. The small errors in the pre-gel region result from the assumptions used to implement the pseudo-kinetic constant and numerical fractionation approaches.

4.3.1. *Effects of diene feed flow rate*

Diene feed flow rate is critical to control the degree of crosslinking reactions and the amount of gel because the crosslinking reaction rate is proportional to the square of the diene content in polymer. Simulation results show that doubling diene feed flow rate without changing other feed flows reduced the critical k_c to 0.23 of its original value; the critical residence time was reduced by a corresponding amount. On the other hand, reducing the diene feed flow rate by one-half increased the critical k_c to 4.12 times its initial value. Therefore, the critical k_c or critical residence time is approximately inversely proportional to the square of the diene feed flow rate. In manufacturing practice, caution must be taken when adjusting diene feed flow rate, in order to avoid excessive gel production.

4.3.2. *Construction of MWD*

An approximate molecular weight distribution can be constructed by assuming each generation obeys a certain distribution function. Here the Schulz two-parameter (Γ) distribution function (Boyd and Phillips, 1993; Teymour and Campbell, 1994) is used,

$$W(x,m) = \frac{y_m (x y_m)^{z_m} \mathrm{e}^{-x y_m}}{\Gamma(z_m + 1)}, \tag{67}$$

where z_m and y_m are defined as

$$z_m = \frac{1}{Pd_m - 1}, \tag{68}$$

$$y_m = \frac{z_m + 1}{\bar{M}_{w,m}}. \tag{69}$$

W is the mass fraction of the mth generation polymer chains with mass x, $\bar{M}_{w,m}$ is the weight average molecular weight of the mth generation polymer, Pd_m is the polydispersity of the mth generation, and Γ represents the gamma function. Using this distribution function, we can reconstruct the MWD of

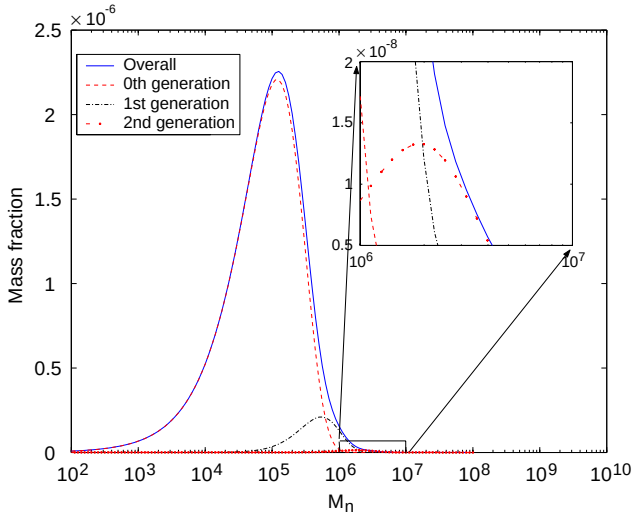

Fig. 9. Molecular weight distribution of the sol at steady state.

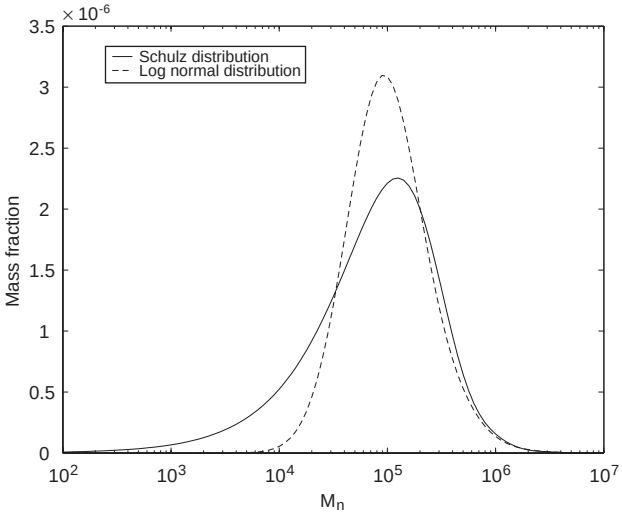

Fig. 10. Comparison of molecular weight distribution of the sol at steady state using a Schulz or log normal distribution in each generation, $k_c/k_{c,c} = 3.12$.

the sol by a weighted sum of the mass fractions $W(x,m)$ of each generation:

$$W(x) = \sum_{m=0}^{M} W(x,m)\frac{g_{m,1}}{B_1}. \tag{70}$$

Fig. 9 shows the MWD at steady state when $\frac{k_c}{k_{c,c}} = 3.12$. The results show that at steady state the sol is primarily composed of linear polymer chains (zeroth generation) and first-generation branched polymer chains. From the enlarged picture at the top right of Fig. 9, we see that the mass fraction of the second generation is small compared to the first two generations. Therefore, the effect of the second and higher generations on the MWD is negligible, and the overall sol distribution is unimodal. This finding differs from that of some other applications of numerical fractionation (Arzamendi and Asua, 1995; Butte et al., 1999; Papavasiliou et al., 2002), where a pronounced shoulder was observed due to artifacts of the method, specifically the third moment closure approximation coupled with the assumption of a Schulz distribution within each generation (Papavasiliou et al., 2002). But in this work, the overall MWD is narrower and closer to a Schulz distribution. For comparison, a log-normal distribution as suggested by Papavasiliou et al. (2002) was incorporated into the model, applying it to each generation. However, it was found that for the log-normal distribution the ODE solver could not converge moments of generations higher than the fifth, while with the Schulz distribution and the same tolerances the moments of all eleven generations converge. A comparison of the MWDs reconstructed using the zeroth through fifth generations is plotted in Fig. 10. Whether based on the Schulz or log normal generational assumptions, neither reconstructed MWD exhibits an artificial shoulder. The MWD reconstructed using the log normal distribution yields a slightly smaller molecular weight at its peak than does the Schulz distribution. The predicted time-dependent polydispersities, at the conditions of Fig. 10, are almost identical except in a narrow region ($t/\theta \sim \pm 0.1$) around the gel point, where they differ by $\sim 15\%$. One cannot choose between the results, because a direct solution cannot be obtained in this region. While recent work postulates that a weighted sum of the two distributions at the generational level can better reproduce direct solution results, these simulations suggest that for this case the results from a weighted sum approach would not differ markedly from those obtained using either (Schulz or log normal distribution) assumption, except at the gel point itself.

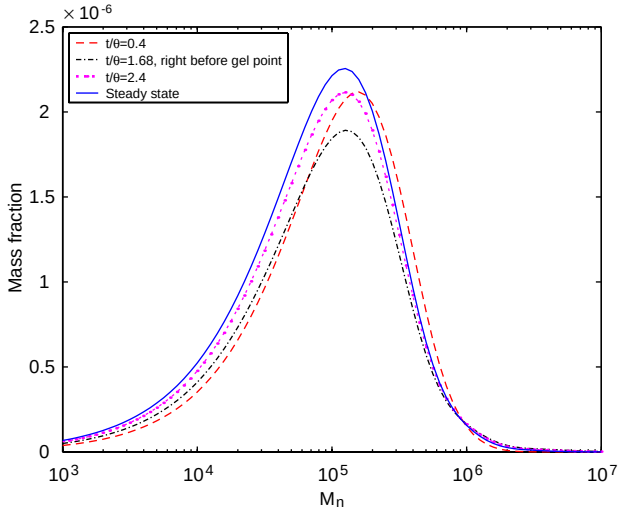

Fig. 11. Evolution of the molecular weight distribution of the sol in the post-gel region.

Fig. 11 shows the sol MWD obtained when $\frac{k_c}{k_{c,c}} = 3.12$ moving from the pre-gel region to the final steady state in the post-gel region. In Fig. 12, the tail area of Fig. 11 is enlarged

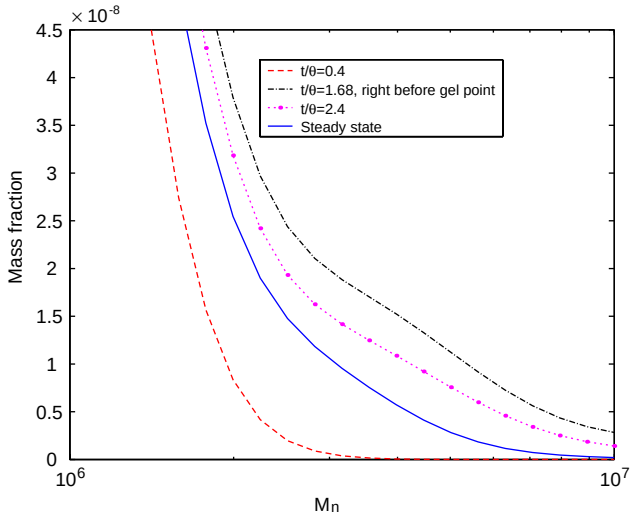

Fig. 12. Evolution of the molecular weight distribution of the sol in the high-molecular weight region.

for better visualization of the changes taking place in the vicinity of the gel point. The shape of this tail region is typical of crosslinked EPDM terpolymers as measured by low angle light scattering (ver Strate, 1985). From the two figures we see that the MWD at startup has the shortest tail because the polymer is still mainly composed of linear chains. As the process approaches the gel point, more generations with high number average molecular weights are formed, shifting the tail to the right. The MWD curve just before the initial gel time has the longest tail because it has the most populated generations. As a result, both the mass fraction of polymer at the MWD maximum and $\bar{M}_n$ itself decrease as the process approaches the gel point. In the post-gel region, the tail is less pronounced because higher generations with higher molecular weights have been consumed as gel.

5. Conclusions

A crosslinking mechanism based on the reaction of pendant double bonds of the diene monomer has been proposed and evaluated for an EPDM terpolymerization process in a CSTR. Computation of the molecular weight distributions under dynamic conditions, in both pre- and post-gel regions, has been performed for a process of this type for the first time. This is made possible by a combination of a numerical fractionation (generational) method along with a pseudo-kinetic constant approach. The assumptions were validated by comparing full model solutions to a reduced model for various limiting cases. In particular, a long-chain assumption causes some error in computing polydispersities near the gel point, but the error decreases rapidly in the post-gel region.

The dynamics of the crosslinking reactions were studied in the post-gel region; number average chain length, polydispersity and sol fraction could be computed with as few as five generations, at reasonable computational expense. The higher generations of the sol are consumed rapidly, causing the sol polydispersity to decrease rapidly to its steady-state value. The largest steady-state sol polydispersity is obtained when the crosslinking rate constant just exceeds a critical value. This critical value is inversely proportional to the second moment of PDBs for the polymer prior to, or in the absence of, crosslinking. The sol polydispersities decrease exponentially with higher values of the rate constant. The first two generations contribute the most to the MWD, which is unimodal. The tail of the MWD is longest near the time of initial gelation; this tail is shortened in the post-gel region as higher generations are consumed as gel.

Notation

B	moment of dead chains, mol/m^3
C	concentration, mol/m^3
F	outlet volumetric flow rate, m^3/s
g	moment of generation, mol/m^3
k	rate constant, s^{-1} or m^3/(mol s)
k_a	rate constant, catalyst activation reaction
k_c	rate constant, crosslinking reaction
k_x	rate constant, spontaneous catalyst deactivation
k_{x_2}	rate constant, catalyst deactivation with propylene
k_{x_3}	rate constant, catalyst deactivation with diene
k_{i1}	rate constant, chain initiation with ethylene
k_{i2}	rate constant, chain initiation with propylene
k_{11}	rate constant, ethylene adding to an ethylene-ended chain
k_{12}	rate constant, propylene adding to an ethylene-ended chain
k_{13}	rate constant, diene adding to an ethylene-ended chain
k_{21}	rate constant, ethylene adding to a propylene-ended chain
k_{22}	rate constant, propylene adding to a propylene-ended chain
k_{31}	rate constant, ethylene adding to a diene-ended chain
k_t	rate constant, spontaneous termination
k_{t_2}	rate constant, termination with propylene
k_{t_3}	rate constant, termination with diene
k_{tr}	rate constant, chain transfer with aluminum alkyl
k_{tr_1}	rate constant, chain transfer with hydrogen
$k_{tr_{M_2}}$	rate constant, chain transfer with propylene
L	moment of live chains, mol/m^3
m_f	molar flow rate of feed, mol/h
M	number of generations used in the simulation
$\bar{M}_n$	number average molecular weight, kg/mol
$\bar{M}_w$	weight average molecular weight, kg/mol

Mw_{av}	monomer average molecular weight, kg/mol
Pd	polydispersity
P	concentration of ethylene ended chains, mol/m^3
PDB	concentration of pendant double bonds in dead chains, mol/m^3
Q	concentration of propylene-ended chains, mol/m^3
R	concentration of diene-ended chains, mol/m^3
r_c	crosslinking reaction rate, mol/(m^3 s)
r_m	monomer consumption rate, mol/(m^3 s)
r_p	propagation reaction rate, mol/(m^3 s)
t	time or age, s
V	volume of the reactor, m^3
W	mass fraction
X	polymer content
x	mass of chains, kg, or mole fraction
y	Schulz distribution variable
z	Schulz distribution variable

Species

Al	aluminum alkyl
C_1	inactive catalyst
C_2	active catalyst
D	dead chain
H_2	hydrogen
M	pseudo-monomer
M_1	monomer 1, ethylene
M_2	monomer 2, propylene
M_3	monomer 3, diene
P	ethylene-ended live chain
PDB	pendant double bond
Q	propylene-ended live chain
R	diene-ended live chain

Greek letters

Γ	gamma function
θ	residence time, h
λ	bulk moment, L/mol
Φ	mole fraction

Subscripts

0	zeroth moment
100	first moment with respect to M_1
010	first moment with respect to M_2
001	first moment with respect to M_3
2	second moment
200	second moment with respect to M_1
020	second moment with respect to M_2
002	second moment with respect to M_3
110	second moment with respect to M_1 and M_2
101	second moment with respect to M_1 and M_3
011	second moment with respect to M_2 and M_3
c	critical value
f	feed
i	the number of M_1 units in the polymer chain
j	the number of M_2 units in the polymer chain
k	the number of M_3 units in the polymer chain
l	the number of pendant double bonds in the polymer chain
L	prior to or in the absence of crosslinking
m	generation
r	the number of monomer units in the polymer chain

Acknowledgements

Financial support from ExxonMobil Chemical Company is gratefully acknowledged. The authors also acknowledge Profs. Fouad Teymour (Illinois Institute of Technology) and John Gossage (Lamar University) for providing valuable information about the numerical fractionation method.

Appendix A. Kinetics mechanism (see Table 3)

Appendix B. Model equations of pseudo-kinetic constant method—standard moment approach

B.1. Components

Concentration of ethylene:

$$\frac{dC_{M_1}}{dt} = \frac{m_{f,M_1}}{V} - \frac{F}{V} C_{M_1} - [k_{i1} C_{C_2} + (k_{11}\Phi_P + k_{21}\Phi_Q + k_{31}\Phi_R) L_0] C_{M_1}. \quad (B.1)$$

Concentration of propylene:

$$\frac{dC_{M_2}}{dt} = \frac{m_{f,M_2}}{V} - \frac{F}{V} C_{M_2} - [k_{x2} C_{C_1} + k_{i2} C_{C_2} + (k_{12}\Phi_P + k_{22}\Phi_Q + k_{t_2} + k_{tr_{M_2}}) L_0] C_{M_2}. \quad (B.2)$$

Concentration of diene:

$$\frac{dC_{M_3}}{dt} = \frac{m_{f,M_3}}{V} - \frac{F}{V} C_{M_3} - [k_{x_3} C_{C_1} + (k_{13}\Phi_P + k_{t_3}) L_0] C_{M_3}. \quad (B.3)$$

Concentration of inactive catalyst:

$$\frac{dC_{C_1}}{dt} = \frac{m_{f,C_1}}{V} - \frac{F}{V} C_{C_1} - (k_a + k_x + k_{x_2} C_{M_2} + k_{x_3} C_{M_3}) C_{C_1}. \quad (B.4)$$

Concentration of active catalyst:

$$\frac{dC_{C_2}}{dt} = \frac{m_{f,C_2}}{V} - \frac{F}{V} C_{C_2} + k_a C_{C_1} - (k_{i1} C_{M_1} + k_{i2} C_{M_2}) C_{C_2} + k_{tr_1} C_{H_2} L_0. \quad (B.5)$$

Table 3
Kinetics mechanism

Type	Reaction	Rate constant
1. Catalyst activation	$C_1 \rightarrow C_2$	k_a
2. Catalyst deactivation	$C_1 \rightarrow D$	k_x
	$C_1 + M_2 \rightarrow D$	k_{x2}
	$C_1 + M_3 \rightarrow D$	k_{x3}
3. Chain initiation	$C_2 + M_1 \rightarrow P_{100}$	k_{i1}
	$C_2 + M_2 \rightarrow Q_{010}$	k_{i2}
4. Chain propagation	$P_{ijk} + M_1 \rightarrow P_{(i+1)jk}$	k_{11}
	$P_{ijk} + M_2 \rightarrow Q_{i(j+1)k}$	k_{12}
	$P_{ijk} + M_3 \rightarrow R_{ij(k+1)}$	k_{12}
	$Q_{ijk} + M_1 \rightarrow P_{(i+1)jk}$	k_{21}
	$Q_{ijk} + M_2 \rightarrow Q_{i(j+1)k}$	k_{22}
	$R_{ijk} + M_1 \rightarrow P_{(i+1)jk}$	k_{31}
5. Chain termination		
Spontaneous	$P_{ijk} \rightarrow U_{ijk}$	k_t
	$Q_{ijk} \rightarrow V_{ijk}$	k_t
	$R_{ijk} \rightarrow W_{ijk}$	k_t
With propylene	$P_{ijk} + M_2 \rightarrow U_{ijk}$	k_{t2}
	$Q_{ijk} + M_2 \rightarrow V_{ijk}$	k_{t2}
	$R_{ijk} + M_2 \rightarrow W_{ijk}$	k_{t2}
With diene	$P_{ijk} + M_3 \rightarrow U_{ijk}$	k_{t3}
	$Q_{ijk} + M_3 \rightarrow V_{ijk}$	k_{t3}
	$R_{ijk} + M_3 \rightarrow W_{ijk}$	k_{t3}
6. Chain transfer		
With hydrogen	$P_{ijk} + H_2 \rightarrow U_{ijk} + C_2$	k_{tr1}
	$Q_{ijk} + H_2 \rightarrow V_{ijk} + C_2$	k_{tr1}
	$R_{ijk} + H_2 \rightarrow W_{ijk} + C_2$	k_{tr1}
With cocatalyst	$P_{ijk} + Al \rightarrow U_{ijk} + P_{100}$	k_{tr}
	$Q_{ijk} + Al \rightarrow V_{ijk} + P_{100}$	k_{tr}
	$R_{ijk} + Al \rightarrow W_{ijk} + P_{100}$	k_{tr}
With propylene	$P_{ijk} + M_2 \rightarrow U_{ijk} + Q_{010}$	k_{trM2}
	$Q_{ijk} + M_2 \rightarrow V_{ijk} + Q_{010}$	k_{trM2}
	$R_{ijk} + M_2 \rightarrow W_{ijk} + Q_{010}$	k_{trM2}

Concentration of hydrogen:

$$\frac{dC_{H_2}}{dt} = \frac{m_{f,H_2}}{V} - \frac{F}{V}C_{H_2} - k_{tr_1}C_{H_2}L_0. \tag{B.6}$$

Concentration of alkyl:

$$\frac{dC_{Al}}{dt} = \frac{m_{f,Al}}{V} - \frac{F}{V}C_{Al} - k_{tr}\left(\frac{C_{Al}}{C_{C_1}} - 1\right)L_0. \tag{B.7}$$

B.2. Zeroth moments

Concentration of live chains:

$$\frac{dL_0}{dt} = \frac{m_{f,P_{0,s}}}{V} - \frac{F}{V}L_0 + (k_{i1}C_{M_1} + k_{i2}C_{M_2})C_{C_2} - [k_t + k_{t_2}C_{M_2} + k_{t_3}C_{M_3} + k_{tr_1}C_{M_2})L_0. \tag{B.8}$$

Concentration of dead chains:

$$\frac{dB_0}{dt} = \frac{m_{f,B_0}}{V} - \frac{F}{V}B_0 + \left[k_t + k_{t_2}C_{M_2} + k_{t_3}C_{M_3} + k_{tr} \times \left(\frac{C_{Al}}{C_{C_1}} - 1\right) + k_{tr_1}C_{H_2} + k_{tr_{M_2}}C_{M_2}\right]L_0 - \frac{1}{2}k_c(\mathrm{PDB})^2. \tag{B.9}$$

B.3. First moments

Concentration of monomers in live chains:

$$\frac{dL_1}{dt} = \frac{m_{f,L_1}}{V} - \frac{F}{V}L_1 + (k_{i1}C_{M_1} + k_{i2}C_{M_2})C_{C_2} + k_pC_ML_0 - \left[k_t + k_{t_2}C_{M_2} + k_{t_3}C_{M_3} + k_{tr_1}C_{H_2} + k_{tr_{M_2}}C_{M_2} + k_{tr} \times \left(\frac{C_{Al}}{C_{C_1}} - 1\right)\right]L_1 + \left[k_{tr}\left(\frac{C_{Al}}{C_{C_1}} - 1\right) + k_{tr_{M_2}}C_{M_2}\right]L_0. \tag{B.10}$$

Concentration of monomers in dead chains:

$$\frac{dB_1}{dt} = \frac{m_{f,B_1}}{V} - \frac{F}{V}B_1 + \left[k_t + k_{t_2}C_{M_2} + k_{t_3}C_{M_3} + k_{tr} \times \left(\frac{C_{Al}}{C_{C_1}} - 1\right) + k_{tr_1}C_{H_2} + k_{tr_{M_2}}C_{M_2}\right]L_1. \tag{B.11}$$

Concentration of diene (PDB) in live chains:

$$\frac{dL_{001}}{dt} = \frac{m_{f,L_{001}}}{V} - \frac{F}{V}L_{001} + k_{13}\Phi_{\mathrm{PDB}}C_{M_3}L_0. \tag{B.12}$$

Concentration of PDB in dead chains:

$$\frac{dPDB}{dt} = \frac{m_{f,\mathrm{PDB}}}{V} - \frac{F}{V}\mathrm{PDB} + \left[k_t + k_{t_2}C_{M_2} + k_{t_3}C_{M_3} + k_{tr}\left(\frac{C_{Al}}{C_{C_1}} - 1\right) + k_{tr_1}C_{H_2} + k_{tr_{M_2}}C_{M_2}\right]L_{001}. - \frac{1}{2}k_c(\mathrm{PDB})^2. \tag{B.13}$$

B.4. Second moments

Live chains:

$$\frac{dL_2}{dt} = \frac{m_{f,L_2}}{V} - \frac{F}{V}L_2 + (k_{i1}C_{M_1} + k_{i2}C_{M_2})C_{C_2} + k_pC_M(L_0 + 2L_1) + \left[(k_{tr}\left(\frac{C_{Al}}{C_{C_1}} - 1\right) + k_{tr_{M_2}}C_{M_2}\right]L_0. \tag{B.14}$$

Dead chains:

$$\frac{dB_2}{dt} = \frac{m_{f,B_2}}{V} - \frac{F}{V}B_2 + \left[k_t + k_{t_2}C_{M_2} + k_{t_3}C_{M_3} + k_{tr} \times \left(\frac{C_{Al}}{C_{C_1}} - 1\right) + k_{tr_{1,s}}C_{H_2} + k_{tr_{M_2}}C_{M_2}\right]L_2. + k_c(\Phi_{\mathrm{PDB}}B_2)^2 \tag{B.15}$$

B.5. Physical properties

B.5.1. Monomer average molecular weight

$$M_{w,\mathrm{av}} = \frac{1}{r_M}\sum_{i=1}^{3} M_{w,M_i} r_{M_i}, \tag{B.16}$$

where r_{M_i} is the monomer consumption rate of the ith monomer:

$$r_{M_1} = (k_{i1}C_{C_2} + k_{11}\Phi_P + k_{21}\Phi_Q + k_{31}\Phi_R)C_{M_1}, \tag{B.17}$$

$$r_{M_2} = [k_{i2}C_{C_2} + k_{12}\Phi_P + k_{22}\Phi_Q + (k_{t_2} + k_{tr_{M_2}})L_0]C_{M_2}, \tag{B.18}$$

$$r_{M_3} = k_{13}\Phi_P + k_{t_3}L_0 C_{M_3}, \tag{B.19}$$

and r_M is the overall monomer consumption rate:

$$r_M = \sum_{i=1}^{3} r_{M_i}. \tag{B.20}$$

The equation for the overall monomer average molecular weight can be derived from the overall mass balance:

$$\frac{\mathrm{d}\bar{M}_{w,\mathrm{av}}}{\mathrm{d}t} = -\frac{F}{V}\bar{M}_{w,\mathrm{av}} + \frac{1}{\lambda_1}\left[R_M M_{w,\mathrm{av}} - \bar{M}_{w,\mathrm{av}} \times \left(\frac{\mathrm{d}L_1}{\mathrm{d}t} + \frac{\mathrm{d}B_1}{\mathrm{d}t}\right)\right]. \tag{B.21}$$

B.5.2. Monomer contents

The two monomer contents can be derived using the individual mass balances.

Ethylene content:

$$\frac{\mathrm{d}X_{M_1}}{\mathrm{d}t} = -\frac{F}{V}X_{M_1} + \frac{1}{\lambda_1\bar{M}_{w,\mathrm{av}}}\left[r_{M_1}M_{w,M_1} - \lambda_1 X_{M_1} \times \frac{\mathrm{d}\bar{M}_{w,\mathrm{av}}}{\mathrm{d}t} - \bar{M}_{w,\mathrm{av}}X_{M_1}\left(\frac{\mathrm{d}L_1}{\mathrm{d}t} + \frac{\mathrm{d}B_1}{\mathrm{d}t}\right)\right]. \tag{B.22}$$

Diene content:

$$\frac{\mathrm{d}X_{M_3}}{\mathrm{d}t} = -\frac{F}{V}X_{M_3} + \frac{1}{\lambda_1\bar{M}_{w,\mathrm{av}}}\left[R_{M_3}M_{w,M_3} - \lambda_1 X_{M_3} \times \frac{\mathrm{d}\bar{M}_{w,\mathrm{av}}}{\mathrm{d}t} - \bar{M}_{w,\mathrm{av}}X_{M_3}\left(\frac{\mathrm{d}L_1}{\mathrm{d}t} + \frac{\mathrm{d}B_1}{\mathrm{d}t}\right)\right]. \tag{B.23}$$

B.5.3. Average molecular weights and polydispersity

Number average molecular weight:

$$\bar{M}_n = \bar{M}_{w,\mathrm{av}}\frac{\lambda_1}{\lambda_0}. \tag{B.24}$$

Weight average molecular weight:

$$\bar{M}_w = \bar{M}_{w,\mathrm{av}}\frac{\lambda_2}{\lambda_1}. \tag{B.25}$$

Polydispersity:

$$\mathrm{Pd} = \frac{\bar{M}_w}{\bar{M}_n} = \frac{\lambda_2\lambda_0}{(\lambda_1)^2}. \tag{B.26}$$

References

Arzamendi, G., Asua, J.M., 1995. Modeling gelation and sol molecular-weight distribution in emulsion polymerization. Macromolecules 28, 7479–7490.

Bank Jr., R.E., Coughran, W.C., Fichtner, W., Grosse, E., Rose, D., Smith, R., 1985. Transient simulation of silicon devices and circuits. IEEE Transaction on Computer-Aided Design 4, 436–451.

Beardsley, K.P., Tomlinson, R.W., 1990. Processing of EPDM polymers as related to structure and rheology. Rubber Chemistry and Technology 63, 540–553.

Beelen, H.J.H., Maag, L.R., Noordermeer, J.W.M., 1998. Understanding the influence of polymer and compounding variations on EPDM extrusions. Rubber World 4, 18–19.

Boyd, R.D., Phillips, P.J., 1993. The Science of Polymer Molecules. Cambridge University Press, Cambridge.

Butte, A., Ghielmi, A., Storti, G., Morbidelli, M., 1999. Calculation of molecular weight distribution in free-radical polymerization with chain branching. Macromolecular Theory and Simulations 8, 498–512.

Cozewith, C., 1988. Transient response of continuous-flow stirred-tank polymerization reactors. A.I.Ch.E. Journal 34, 272–282.

Cozewith, C., Teymour, F., 1998. Polymer cross-linking in post-gel region for continuous and batch reactors. A.I.Ch.E. Journal 44, 722–732.

Cozewith, C., Graessley, W.W., ver Strate, G., 1979. Polymer cross-linking in continuous flow stirred reactors. Chemical Engineering Science 34, 245–248.

Dikland, H.G., 1996. Influence of chemical composition and molecular structure of EPDM on peroxide crosslinking efficiency. Kautschuk Gummi Kunstoffe 49, 413–417.

Dolatkhani, M., Cramail, H., Deffieux, A., 1996. Linear non-conjugated dienes from biomass as termonomers in EPDM synthesis, 2: Comparison with 5-ethylidene-2-norbornene termonomer. Macromolecular Chemistry and Physics 197, 289–302.

Flory, P.J., 1953. Principles of Polymer Chemistry. Cornell University Press, New York.

Gardner, I.J., ver Strate, G., 1973. Determination of ethylidenenorbornene in EPDM terpolymers. Rubber Chemistry and Technology 46, 1019–1034.

Gossage, J.L., 1997. Numerical fractionation modeling of nonlinear polymerization. Ph.D. Thesis, Illinois Institute of Technology, Chicago, IL, USA.

Kennedy, J.P., Makowski, H.S., 1967. Carbonium ion polymerization of norbornene and its derivatives. Macromolecular Science (Chemistry) A1, 345–370.

Kresge, E.N., Cozewith, C., ver Strate, G., 1985. Long chain branching and gel in EPDM. Rubber Chemistry and Technology 58, 180–181.

Mazzotti, M., Fiorentino, S., Ghielmi, A., 1996. Kinetics of long-chain branching in emulsion polymerization. Macromolecular Symposia 111, 183–193.

Noordermeer, J.W.M., 1997. Standardization of EPDM characterization tests for QC and specification purposes. Rubber World 217, 16–20.

Office of Air Quality, 1995. Hazardous air pollutant emissions from process units in the elastomer manufacturing industry—basis and purpose document for proposed standards. Tech. Rep.EPA-453/R-95-006a, Environmental Protection Agency.

Ogunnaike, B.A., 1994. On-line modelling and predictive control of an industrial terpolymerization reactor. International Journal of Control 59, 711–729.

Papavasiliou, G., Birol, I., Teymour, F., 2002. Calculation of molecular weight distribution in non-linear free-radical polymerization using the numerical fractionation technique. Macromolecular Theory and Simulations 11, 533–548.

Pehlert, G.J., Dharmarajan, N.R., Ravishankar, P.S., 2001. Blends of EP(D)M and metallocene plastomers for wire and cable applications. 159th Meeting, ACS Rubber Division, Providence, RI, USA.

Pladis, P., Kiparissides, C., 1998. A comprehensive model for the calculation of molecular weight long-chain branching distribution in free-radical polymerizations. Chemical Engineering Science 53, 3315–3333.

Saatkamp, T., Lechner, M.D., Otten, M., Vennemann, N., 1995. Comparison of technological test procedures for the characterization of processing behavior. Kautschuk Gummi Kunstoffe 12, 892–896.

Saidel, G.M., Katz, S., 1968. Dynamic analysis of branching in radical polymerization. Polymer Science: Polymer Physics Edition 6, 1149–1160.

Shaffer, W.K.A., Ray, W.H., 1997. Polymerization of olefins through heterogeneous catalysis. XVIII. A kinetic explanation for unusual effects. Journal of Applied Polymer Science 65, 1053–1080.

Shampine, L.F., Hosea, M.E., 1996. Analysis and implementation of TR-BDF2. Applied Numerical Mathematics 20, 21–37.

Teymour, F., Campbell, J.D., 1994. Analysis of the dynamics of gelation on polymer reactors using the "numerical fractionation" technique. Macromolecules 27, 2460–2469.

Topalis, E., Pladis, P., Kiparissides, C., Goossens, I., 1996. Dynamic modelling and steady-state multiplicity in high pressure multizone LDPE autoclaves. Chemical Engineering Science 51, 2461–2470.

ver Strate, G., 1985. Ethylene–propylene elastomers. In: Mark, H.F., Kroschwitz, J.I. (Eds.), Encyclopedia of Polymer Science and Engineering, 2nd Edition, Vol. 6. Wiley, New York, pp. 522–564.

ver Strate, G., Cozewith, C., Graessley, W.W., 1980. Branching by copolymerization of monovinyl and divinyl monomers in continuous-flow stirred reactors. Journal of Applied Polymer Science 25, 59–62.

Xie, T., Hamielec, A.E., 1993a. Modeling free-radical copolymerization kinetics—evaluation of the pseudo-kinetic rate constant method. 1 Molecular weight calculations for linear copolymers. Makromolekulare Chemie—Theory and Simulations 2, 421–454.

Xie, T., Hamielec, A.E., 1993b. Modeling free-radical copolymerization kinetics—evaluation of the pseudo-kinetic rate constant method. 2 Molecular weight calculations for copolymers with long chain branching. Makromolekulare Chemie—Theory and Simulations 2, 455–483.

Xie, T., Hamielec, A.E., 1993c. Modeling free-radical copolymerization kinetics—evaluation of the pseudo-kinetic rate constant method. 3 Molecular weight calculations for copolymers with crosslinking. Makromolekulare Chemie—Theory and Simulations 2, 777–803.